

# Mechanosynthesis as a Simple Method to Obtain a Magnetic Composite (Activated Carbon/Fe<sub>3</sub>O<sub>4</sub>) for Hyperthermia Treatment

Jorge Carlos Ríos-Hurtado<sup>1</sup>, Elia Martha Múzquiz-Ramos<sup>1\*</sup>, Alejandro Zugasti-Cruz<sup>1</sup>,  
Dora Alicia Cortés-Hernández<sup>2</sup>

<sup>1</sup>Facultad de Ciencias Químicas, Universidad Autónoma de Coahuila, Saltillo, México

<sup>2</sup>Centro de Investigación y de Estudios Avanzados del Instituto Politécnico Nacional Unidad Saltillo,  
Ramos Arizpe, México

Email: [jorge.rios@uadec.edu.mx](mailto:jorge.rios@uadec.edu.mx), [emuzquiz@uadec.edu.mx](mailto:emuzquiz@uadec.edu.mx)

Received 18 November 2015; accepted 3 January 2016; published 6 January 2016

Copyright © 2016 by authors and Scientific Research Publishing Inc.

This work is licensed under the Creative Commons Attribution International License (CC BY).

<http://creativecommons.org/licenses/by/4.0/>



Open Access

---

## Abstract

A large number of magnetic nanomaterials have been studied for their hyperthermic potential, such as iron oxide based materials. These are embedded in different matrices to improve their properties. In this paper magnetite was synthesized by the coprecipitation method and an activated carbon/magnetite composite was obtained by mechanosynthesis (400 rpm, 3 h). The samples were characterized by X-ray diffraction (XRD), vibrating sample magnetometer (VSM), IR-FT spectroscopy and Scanning Electron Microscopy (SEM). Furthermore, composite heating curves as well as hemolysis tests were performed. The composite showed a superparamagnetic behavior due to its low coercivity index (8.92 Oe) and a high saturation magnetization (40.12 emu/g). SEM images showed that the magnetite was observed on the surface of activated carbon and also the IR-FT spectra indicated that oxygenated groups on the activated carbon surface were responsible for the anchoring of magnetite in the surface, with particle sizes between 9 and 14 nm. Heating results indicated that a composite mass of 18 mg reach a temperature of 45.6°C in a low frequency magnetic field (10.2 kA and 200 kHz). Hemolysis tests indicated that the composite is a non-hemolytic material (4.7% hemolysis). These results demonstrate that the material can be used in magnetic hyperthermia techniques for cancer treatment.

## Keywords

Mechanosynthesis, Hyperthermia, Magnetite, Activated Carbon, Composite

---

\*Corresponding author.

## 1. Introduction

Magnetic nanoparticles offer some attractive possibilities in biomedicine. Firstly, they have controllable sizes ranging from a few nanometers up to ten nanometers, which place them at dimensions that are smaller than or comparable to different human body components. Secondly, the nanoparticles obey Coulomb's law, and can be manipulated by an external magnetic field gradient. Thirdly, the magnetic nanoparticles can be made to resonantly respond to a time-varying magnetic field, with advantageous results related to the transfer of energy from the exciting field to the nanoparticle [1].

This last feature makes the magnetic nanoparticles able to heat up leading to their potential use as hyperthermia agents. Magnetic hyperthermia has recently attracted significant attention as a safe method for cancer therapy. It can increase the temperature in tumors to 41°C - 46°C, thereby killing the tumor cells with minimum damage to normal tissue [2].

Nano-magnetic particles with tailored surface chemistry have been widely used experimentally for numerous *in vivo* applications such as hyperthermia, magnetic resonance imaging (MRI) contrast agent, tissue repair, immunoassay, drug delivery, and cell separation [3]. The concept of magnetically mediated heating of iron-oxide nanoparticles is gaining increasing attention as a potential new cancer treatment [4]. The heating of oxide magnetic materials with low electrical conductivity in an external alternating magnetic field is due to loss processes during the reorientation of the magnetization [5].

Among various magnetic nanoparticles, magnetite ( $\text{Fe}_3\text{O}_4$ ) has been considered suitable due to its biocompatibility, ease of synthesis and heating properties [6]. Iron oxide nanoparticles have been synthesized by hydrothermal method [7], hydrolysis [8], sol-gel assisted electrospinning [9], vapor-liquid-solid growth [10], a solvothermal synthesis [11], thermolysis [12], a wet chemical process [13], flame synthesis [14], etc. However, coprecipitation is often employed because nanoparticles with uniform phase can be obtained and the synthesis processes such as reaction, washing and solid-liquid separation are simple [15].

Moreover, the use of different matrix such polymers [16]-[19] and ceramics materials [20]-[24] to transport the nanoparticles into the body has been researched. The ability to manipulate/bind individual molecules at nanoscale has provided ample opportunity for new therapeutic and diagnostic applications. In this way, nanocomposites can be obtained or it may be embedded in biocompatible materials to impart new functionalities. Activated carbon is a good choice as a coating, due to its high surface area and known adsorption-desorption properties for many molecules including peptides, proteins and drugs [25]. The magnetic materials in activated carbon nanocomposites are better to be higher saturation magnetization (Ms) and less concentration for keeping considerably good adsorption performance [26].

The aim of this work was to synthesize a magnetic composite using activated carbon with magnetite, so that being within the human body and contacting with an external magnetic field, is viable for its use for cancer treatment by magnetic hyperthermia technique.

## 2. Experimental

### 2.1. Activated Carbon Oxidation

The procedure was followed according to established by Rangel-Mendez and Streat in 2001 [27]. 5 g of activated carbon (AC) was placed in a three-necked flask with a solution of  $\text{HNO}_3$  with deionized water (50:50) and this was brought to a controlled temperature of 85°C for 3 h. After the respective time, three-necked flask was removed and placed in an ice bath to prevent oxidation further progress. The nitric acid excess was removed and the activated carbon was washed with deionized water. Finally, the activated carbon was dried in an oven at a temperature of 80°C for 24 h.

### 2.2. Obtention of $\text{Fe}_3\text{O}_4$ Nanoparticles

For the synthesis of this ferrite,  $\text{FeCl}_2 \cdot 4\text{H}_2\text{O}$  and  $\text{FeCl}_3 \cdot 6\text{H}_2\text{O}$  (molar ratio 1:2) were mixed in 50 mL of deionized water. On the other hand, in a ball flask were placed 150 mL of deionized water and heated at 70°C at 1000 rpm using a mechanical stirrer.

As the temperature was reached, 50 ml of concentrated ammonium hydroxide (pH 9.8) were added in order to facilitate a basic medium in the solution with low stirring and heating to a temperature of 70°C. Subsequently, mixture of iron chloride solution was added dropwise and left under constant stirring (5000 rpm) for half an

hour.

Once the time has expired, the precipitate obtained was washed with 2 L of deionized water to remove excess chloride and allowed to dry at room temperature for 3 days. Finally, the product obtained was washed with 1 L of water and 250 mL of ethanol and allowed to dry at room temperature.

### 2.3. AC/Fe<sub>3</sub>O<sub>4</sub> Composite Mechanosynthesis

Once obtained magnetite and the oxidized activated carbon, a carbon-magnetite composite (AC/Fe<sub>3</sub>O<sub>4</sub>) was obtained by mechanosynthesis technique. This procedure took place on the FRITSCH planetary mill brand, model Pulverisette 6. A certain amount of activated carbon and ferrite were added to the container and placed in agate mill at 400 rpm for 3 h in order to obtain a composite of ferrite and activated carbon 60%/40% respectively, due to this ratio showed the best heating properties obtained in preliminary tests, since the ferrite mediate the heating capacity. Finally, the product was washed with deionized water and allowed to dry at room temperature.

### 2.4. Materials Characterization

The magnetite nanoparticles and the composite AC/Fe<sub>3</sub>O<sub>4</sub> were analyzed by X-ray diffraction (XRD) (Siemens Mod. D-5000). The magnetic properties of the samples were measured with a SQUID Quantum Design magnetometer (VSM) in applied fields from -12.5 to 12.5 KOe. The particle size and shape were studied by field emission scanning electron microscopy (SEM) (JOEL JSM-7401F) and energy dispersive X-ray (EDX) techniques. FT-IR spectra of the materials have been taken by a Perkin Elmer FTIR, model Spectrometer Frontier.

### 2.5. Heating Capacity

This technique was performed to determine whether the particles had the ability to generate heat. These tests consisted of placing certain concentration of sample, in a vial with 2 mL of water, which was stirred with a vortex. These vials were carried to an equipment of magnetic induction in solid state, which was programmed using a magnetic field (10.2 kA/m and frequency 200 kHz), during 15 minutes.

### 2.6. *In Vitro* Hemolysis Assay

In order to determine the biocompatibility of activated carbon and AC/Fe<sub>3</sub>O<sub>4</sub> composite with human erythrocytes, hemolysis tests were performed. The hemolysis test was performed using human whole blood from healthy non-smoking donors, following the proper guidelines for studies using human specimens. The procedure was conducted as reported by Muzquiz-Ramos *et al.* in 2014 [28]. A certain amount of activated carbon and composite (AC/Fe<sub>3</sub>O<sub>4</sub>) were contacted with 150 µL of human blooderythrocytes in 1850 µL of Alsever's solution (dextrose 0.116 M, NaCl 0.071 M, sodium citrate 0.027 M and citric acid 0.002 M, pH 6.4) in order to obtain concentrations of 0.5 mg/mL, 2 mg/mL and 3 mg/mL. The hemolysis percent was obtained by the Equation (1).

$$\text{Hemolysis \%} = \frac{(A_s - A_c^{[-]})}{(A_c^{[+]} - A_c^{[-]})} \times 100 \quad (1)$$

where:

$A_s$ : Sample absorbance;

$A_c^{[-]}$ : Negative control absorbance (erythrocytes/Alsever's solution);

$A_c^{[+]}$ : Positive control absorbance (erythrocytes/deionized water).

## 3. Results and Discussions

### 3.1. Structural Properties

XRD patterns of magnetite and the AC/Fe<sub>3</sub>O<sub>4</sub> composite are shown in **Figure 1**. The diffraction peaks of the synthesized magnetite in **Figure 1(a)** can be perfectly indexed to the inverse spinel structure (JCPDS card no. 019-0629), and no characteristic peaks of impurities are detected in the XRD pattern, implying that the formation of the single phase spinel. As shown in **Figure 1(b)**, for AC/Fe<sub>3</sub>O<sub>4</sub> composite, could observe the most intense

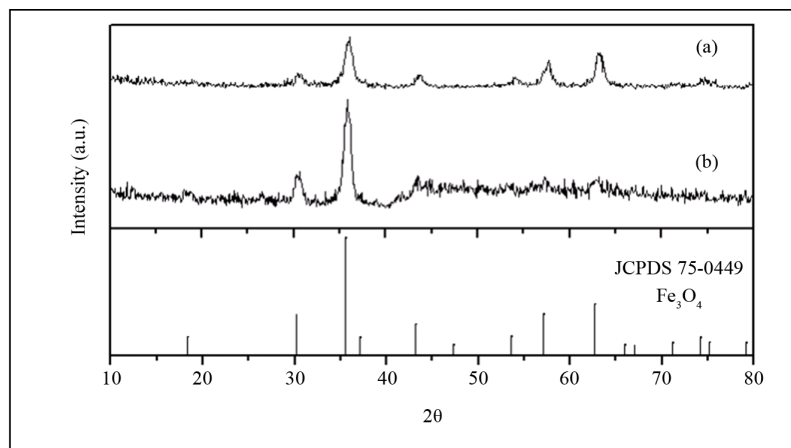


**Figure 1.** XRD patterns of synthesized magnetite (a) and AC/Fe<sub>3</sub>O<sub>4</sub> composite (b); and the reference data for Fe<sub>3</sub>O<sub>4</sub> of the JCPDS file No. 16-0629.

peaks of magnetite. However, it has also been shown that activated carbon has a very broad peak between 40° and 60°, peak that can be observed slightly in the composite XRD pattern. The disappearance of the other peaks may be due to overlap of signals by the amorphous structure of graphite [29].

Furthermore, the crystallite size values were calculated by the Scherrer's equation, taking the most intense peak and the Gaussian model. The crystallite size of the synthesized magnetite is 10.9 nm. Determining the particle size is very useful because, to use a material in magnetic hyperthermia, it must have a size between 9 and 15 nm. It has been shown that the spherical type nano-sized particles have higher diffusion speed, increasing the concentration of nanoparticles in the center of a blood vessel, thus limiting interaction of the nanoparticles with endothelial cells and prolong circulation time of the nanoparticles in the blood [30].

The morphology of the AC/Fe<sub>3</sub>O<sub>4</sub> composite was investigated by SEM observations and EDX analysis. As shown in **Figure 2(a)**, EDX analysis indicates presence of phosphorus in activated carbon surface related to phosphates due to the activation process. Furthermore, in **Figure 2(b)**, it can be seen the composite AC/Fe<sub>3</sub>O<sub>4</sub> micrograph where Fe<sub>3</sub>O<sub>4</sub> particles seem to be deposited on activated carbon surface. Also the EDX analysis indicates a decrease in the amount of C atoms on the composite, in comparison with the activated carbon and moreover the presence of Fe atoms.

In addition, **Figure 3** shows the nanoparticles deposited in activated carbon surface, which have a size between 8 and 22 nm. These results are comparable to those obtained by the Scherrer's equation of crystallite size using the diffraction data.

### 3.2. Magnetic Properties

The magnetic properties of the samples were measured in a SQUID Quantum Design magnetometer in applied fields from -12.5 to 12.5 KOe. **Figure 4** shows the hysteresis loops of the synthesized magnetite (a) and AC/Fe<sub>3</sub>O<sub>4</sub> composite (b). Both hysteresis loops exhibit a superparamagnetic behavior, however the results of saturation magnetization, remanent magnetization and coercivity are summarized in **Table 1**. Coercivity data are of great importance, as these show superparamagnetic behavior of the materials when coercivity values are near 0. In case of the synthesized magnetite coercivity value is 10.28 Oe and for AC/Fe<sub>3</sub>O<sub>4</sub> composite coercivity value is 8.92 Oe. This coercivity values indicates that both samples have a superparamagnetic behavior.

Moreover, the saturation magnetization of AC/Fe<sub>3</sub>O<sub>4</sub> composite decreases in comparison of the synthesized magnetite due to the presence of activated carbon, which has no magnetic properties. These results are consistent with those expected due to the presence of activated carbon, which does not show a magnetic behavior. Mendes *et al.* in 2014, attribute this difference in saturation magnetization due to the presence of a non-magnetic phase, for example an organic diamagnetic material as the activated carbon [31].

### 3.3. Chemical Properties

In order to determine the bonds formed between AC and Fe<sub>3</sub>O<sub>4</sub> in the mechanosynthesis process, infrared

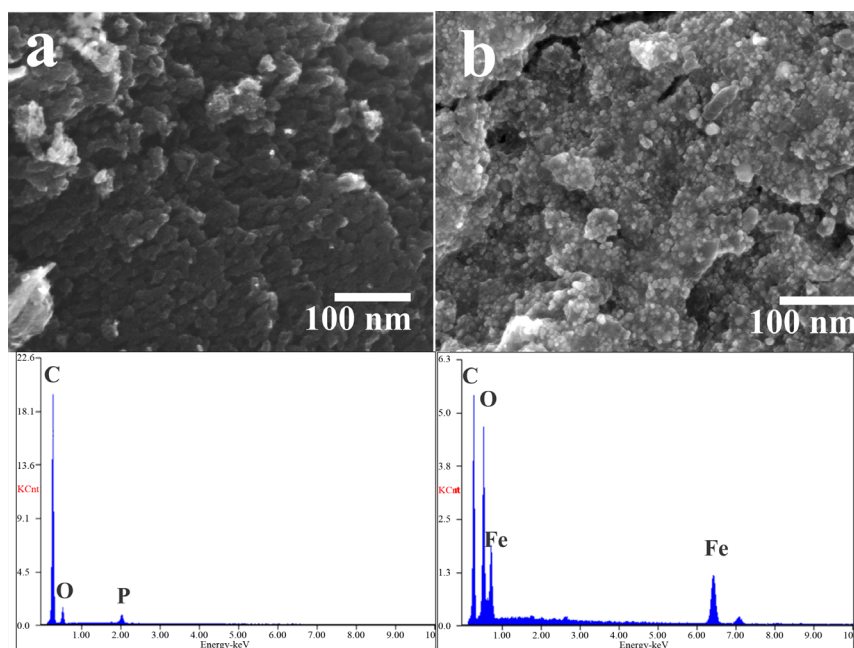


**Figure 2.** SEM micrographs and EDX spectrum. (a) AC and (b) AC/Fe<sub>3</sub>O<sub>4</sub> composite.

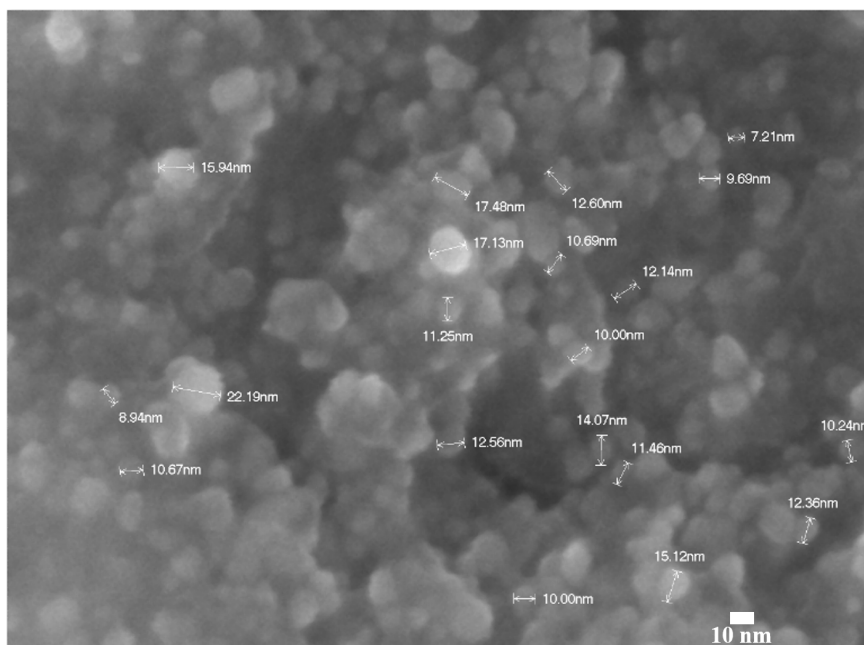


**Figure 3.** SEM micrograph and magnetite particles measurement in AC/Fe<sub>3</sub>O<sub>4</sub> composite (300000 $\times$ ).

spectroscopy tests were performed. FT-IR spectra of oxidized activated carbon (AC) and AC/Fe<sub>3</sub>O<sub>4</sub> composite are shown in **Figure 5**. When activated carbon is contacted with an oxidizing agent such as nitric acid, it has been determined that the concentration of functional groups is increased [32]. Furthermore, also in **Figure 4** it is possible to observe FT-IR spectra of AC/Fe<sub>3</sub>O<sub>4</sub> composite in which there is clearly a decrease in the intensity of the bands between 1500 cm<sup>-1</sup> and 1700 cm<sup>-1</sup> and disappearance of OH<sup>-</sup> band (between 3500 cm<sup>-1</sup> to 3000 cm<sup>-1</sup>), relative to AC precursor. This may indicate that magnetite is being bound to these functional groups in mechano-synthesis process due to the high energy formed in the milling. It is also clear oxygen-metal bond, since a

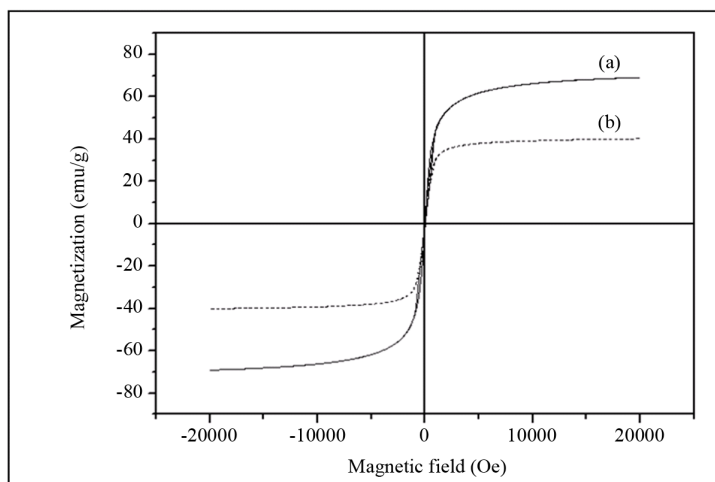


**Figure 4.** Hysteresis loops of the synthesized magnetite (a) and AC/Fe<sub>3</sub>O<sub>4</sub> composite (b).

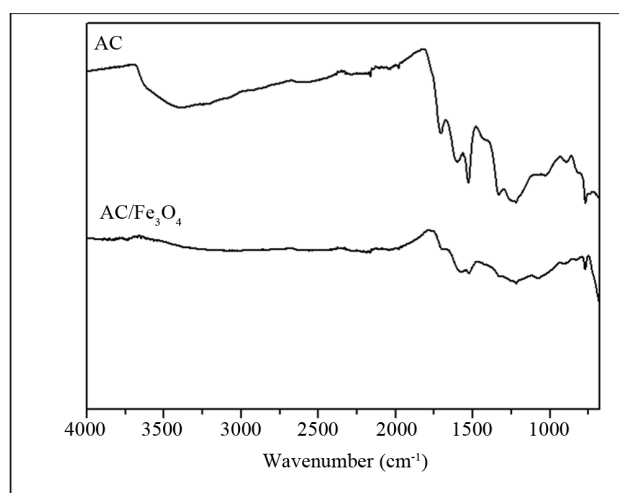


**Figure 5.** FT-IR spectra of activated carbon (AC) and activated carbon/magnetite composite (AC/Fe<sub>3</sub>O<sub>4</sub>).

**Table 1.** Magnetic properties of the synthesized samples.

Sample	Magnetic properties		
	Magnetization $M_s$ (emu/g)	Remanence $M_r$ (emu/g)	Coercivity $H_c$ Oe
Fe <sub>3</sub> O <sub>4</sub>	69.16	0.45	10.28
AC/Fe <sub>3</sub> O <sub>4</sub>	40.12	0.35	8.92

band at 773 cm<sup>-1</sup> is presented.

Moreover, the main functional groups that can be observed in the FT-IR spectra are summarized in **Table 2**, which for activated carbon principal bands attribution are phenolics and carboxylic acid groups, formed by the oxidation process in the material surface. For AC/Fe<sub>3</sub>O<sub>4</sub> composite is more clearly detailed the disappearance of phenolic groups corresponding to bands and some kind of carboxylic acid bond, due to the bond formed between this oxygenated groups and the magnetite.

### 3.4. Heating Capacity

Furthermore, the heating ability of the composite was also tested. Analysis for different masses of AC/Fe<sub>3</sub>O<sub>4</sub>

composite (16 mg, 18 mg and 20 mg) were performed. Heating curves are presented in **Figure 6**, where the greater the amount of mass greater heating capacity was observed. However, for the mass of 20 mg, this composite managed to generate a temperature of 48.7°C, temperature at which cell damage occurs known as heat ablation. According to the heating curve, 18 mg of the AC/Fe<sub>3</sub>O<sub>4</sub> composite is able to use in hyperthermia technique, since this mass generated a temperature of 45.6°C in 15 minutes. The adequate temperature for hyperthermia treatment it's above 46°C [33].

### 3.5. Biocompatibility Test

For determine if the materials were biocompatible to human erythrocytes, hemolysis assay were carried out. This test is important since the material can be applied directly to the bloodstream, so that in a given moment be in contact with the erythrocytes of a human blood. **Figure 7** shows the hemolysis percent caused by the AC/Fe<sub>3</sub>O<sub>4</sub> composite at different concentrations. Activated carbon hemolysis percent is also reported. Error bars represent the mean and standard deviation for six experiments. The results of hemolytic test (**Figure 7**) demonstrated that the HR of the samples were lower than 5%. According to ASTM F 756-08 (Standard Practice for Assessment of Hemolytic Properties of Materials) [34], HR < 5% produced by any material could be considered as not hemolytic. According to these results, we can deduce that the activated carbon and the composite AC/Fe<sub>3</sub>O<sub>4</sub> are not a hemolytic materials and is biocompatible with human blood erythrocytes.

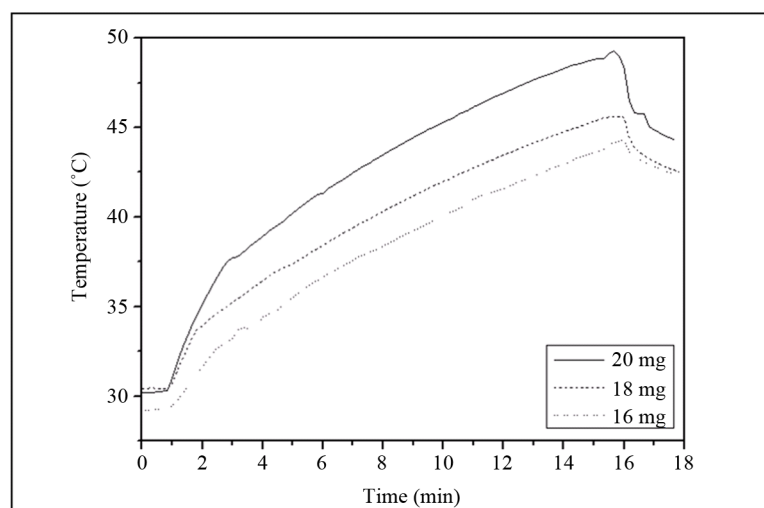


**Figure 6.** Heating curves for different mass of the composite AC/Fe<sub>3</sub>O<sub>4</sub>.

**Table 2.** FT-IR spectra bands observed in the samples.

Sample	FT-IR data		
	Peak (cm <sup>-1</sup> )	Bond	Attribution
AC	3391	-OH	Phenol (graphitic structure)
	1709	-C=O	Saturated carboxylic acid
	1530	-OH	Carboxylic acid
	1221	-COOH	Carboxylic acid
	771	-O-M	Metal-oxygen (impurities)
AC/Fe <sub>3</sub> O <sub>4</sub>	1704	-C=O	Saturated carboxylic acid
	1578	-OH	Carboxylic acid
	1220	-COOH	Carboxylic acid
	773	-O-M	Metal-oxygen (magnetite)

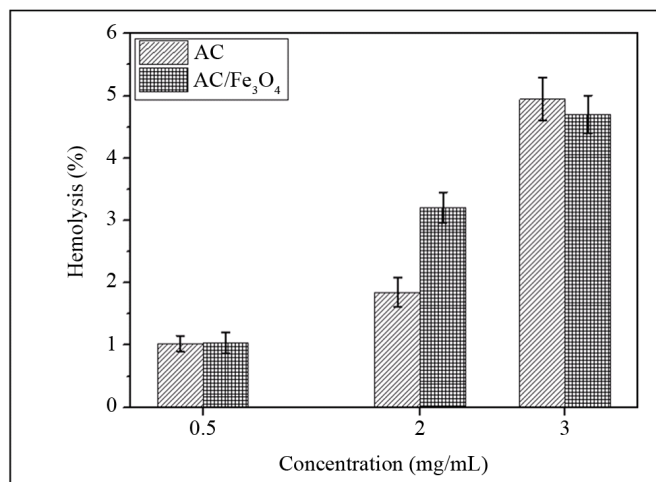


**Figure 7.** Hemolysis (%) caused by AC (lines) and AC/Fe<sub>3</sub>O<sub>4</sub> (square).

#### 4. Conclusion

Activated carbon/magnetite composite was obtained by a simple mechanosynthesis method (400 rpm, 3 h). A superparamagnetic behavior is observed in the composite AC/Fe<sub>3</sub>O<sub>4</sub>. Magnetite particles are on the surface of the activated carbon according to the observed in the SEM images, with a particle size between 9 - 14 nm. The decrease in intensity of bands of oxygenated surface groups of activated carbon in the FT-IR spectra, may indicate that ferrites have been attached to these groups. Moreover, the composite AC/Fe<sub>3</sub>O<sub>4</sub> demonstrated a heat generation of 45.6°C under a low frequency magnetic field. Furthermore, hemolysis tests indicated that AC/Fe<sub>3</sub>O<sub>4</sub> is a non-hemolytic material, since the hemolysis percent was under 5%. The results show that the composite might be used for cancer treatment by magnetic hyperthermia therapy.

#### Acknowledgements

Authors gratefully acknowledge CONACyT-México for the provision of J.C. Ríos-Hurtado scholarship (423185) and SEP (PROFOCIE 2014 project) for the financial support on this research. The authors also thank S.G. Solís-Rosales and J.A. Cepeda-Garza from CIQA for their valuable technical and professional assistance. Finally, authors appreciate the financial support of CGEPI UAdeC for publishing this article.

#### References

- [1] Pankhurst, Q., Connolly, J., Jones, S. and Dobson, J. (2003) Applications of Magnetic Nanoparticles in Biomedicine. *Journal of Physics D: Applied Physics*, **36**, R167. <http://dx.doi.org/10.1088/0022-3727/36/13/201>
- [2] Li, Z., Kawashita, M., Araki, N., Mitsumori, M., Hiraoka, M. and Doi, M. (2011) Preparation of Magnetic Iron Oxide Nanoparticles for Hyperthermia of Cancer in a FeCl<sub>2</sub>-NaNO<sub>3</sub>-NaOH Aqueous System. *Journal of Biomaterials Applications*, **25**, 643-661. <http://dx.doi.org/10.1177/0885328209351136>
- [3] Kim, D., Lee, S., Im, K., Kim, K., Shim, I., Lee, M. and Lee, Y. (2006) Surface-Modified Magnetite Nanoparticles for Hyperthermia: Preparation, Characterization, and Cytotoxicity Studies. *Current Applied Physics*, **6**, e242-e246. <http://dx.doi.org/10.1016/j.cap.2006.01.048>
- [4] Johannsen, M., Gneveckow, U., Eckelt, L., Feussner, A., Waldofner, N., Scholz, R., Deger, S., Wust, P., Loening, S. and Jordan, A. (2005) Clinical Hyperthermia of Prostate Cancer Using Magnetic Nanoparticles: Presentation of a New Interstitial Technique. *International Journal of Hyperthermia*, **7**, 637-647. <http://dx.doi.org/10.1080/02656730500158360>
- [5] Hiergeist, R., Andra, W., Buske, N., Hergt, R., Hilger, I., Richter, U. and Kaiser, W. (1999) Application of Magnetite Ferrofluids for Hyperthermia. *Journal of Magnetism and Magnetic Materials*, **201**, 420-422. [http://dx.doi.org/10.1016/S0304-8853\(99\)00145-6](http://dx.doi.org/10.1016/S0304-8853(99)00145-6)
- [6] Kikuchi, T., Kasuya, R., Endo, S., Nakamura, A., Takai, T., Metzler-Nolte, N., Tohji, K. and Balachandran, J. (2011) Preparation of Magnetite Aqueous Dispersion for Magnetic Fluid Hyperthermia. *Journal of Magnetism and Magnetic*

- Materials*, **323**, 1216-1222. <http://dx.doi.org/10.1016/j.jmmm.2010.11.009>
- [7] Li, Z., Lai, H., Wang, D., Mao, C. and Xing, D. (2009) Direct Hydrothermal Synthesis of a Single-Crystalline Hematite Nanorods Assisted by 1,2-Propanediamine. *Nanotechnology*, **20**, Article ID: 245603. <http://dx.doi.org/10.1088/0957-4484/20/24/245603>
- [8] Lian, S., Wang, E., Kang, Z., Bai, Y., Gao, L., Jiang, M., Hu, C. and Xu, L. (2004) Synthesis of Magnetite Nanorods and Porous Hematite Nanorods. *Solid State Communications*, **129**, 485-490. <http://dx.doi.org/10.1016/j.ssc.2003.11.043>
- [9] Barakat, N. (2012) Synthesis and Characterization of Maghemite Iron Oxide ( $\gamma$ -Fe<sub>2</sub>O<sub>3</sub>) Nanofibers: Novel Semiconductor with Magnetic Feature. *Journal of Materials Science*, **47**, 6237-6245. <http://dx.doi.org/10.1007/s10853-012-6543-7>
- [10] Morber, J., Ding, Y., Haluska, M., Li, Y., Liu, J., Wang, Z. and Snyder, J. (2006) PLD-Assisted VLS Growth of Aligned Ferrite Nanorods, Nowires, and Nanobelts—Synthesis and Properties. *Journal of Physical Chemistry B*, **110**, 21672-21679. <http://dx.doi.org/10.1021/jp064484j>
- [11] Li, Y., Jiang, R., Liu, T. and Lv, H. (2014) Single-Microemulsion-Based Solvothermal Synthesis of Magnetite Microflowers. *Ceramics International*, **40**, 4791-4795. <http://dx.doi.org/10.1016/j.ceramint.2013.09.025>
- [12] Chaudhari, N., Warule, S., Muduli, S., Kale, B., Jouen, S., Lefez, B., Hannover, S. and Ogale, S. (2011) Maghemite (Hematite) Core (Shell) Nanorods via Thermolysis of a Molecular Solid of Fe-Complex. *Dalton Transactions*, **40**, 8003-8011. <http://dx.doi.org/10.1039/c1dt10319a>
- [13] Chen, S., Feng, J., Guo, X., Hong, J. and Ding, W. (2005) One-Step Wet Chemistry for Preparation of Magnetite Nanorods. *Materials Letters*, **59**, 985-988. <http://dx.doi.org/10.1016/j.matlet.2004.11.043>
- [14] Merchan-Merchan, W., Saveliev, A.V. and Taylor, A.M. (2008) High Rate Flame Synthesis of Highly Crystalline Iron Oxides Nanorods. *Nanotechnology*, **19**, Article ID: 125605. <http://dx.doi.org/10.1088/0957-4484/19/12/125605>
- [15] Iwasaki, T., Kosaka, K., Mizutani, N., Watano, S., Yanagida, T., Tanaka, H. and Kawai, T. (2008) Mechanochemical Preparation of Magnetite Nanoparticles by Coprecipitation. *Materials Letters*, **62**, 4155-4157. <http://dx.doi.org/10.1016/j.matlet.2008.06.034>
- [16] Balakrishnan, S., Bonder, M. and Hadjipanayis, G. (2009) Particle Size Effect on Phase and Magnetic Properties of Polymer-Coated Magnetic Nanoparticles. *Journal of Magnetism and Magnetic Materials*, **321**, 117-122. <http://dx.doi.org/10.1016/j.jmmm.2008.08.055>
- [17] Castrejón-Parga, K., Camacho-Montes, H., Rodríguez-González, C., Velasco-Santos, C., Martínez-Hernández, A., Bueno-Jaquez, D., Rivera-Armenta, J., Ambrosio, C., Chapa, C., Mendoza-Duarte, M. and García-Casillas, P. (2014) Chitosan-Starch Film Reinforced with Magnetite-Decorated Carbon Nanotubes. *Journal of Alloys and Compounds*, **615**, 5505-5510. <http://dx.doi.org/10.1016/j.jallcom.2013.12.269>
- [18] Kadar, E., Batalha, I., Fisher, A. and Roque, A. (2014) The Interaction of Polymer-Coated Magnetic Nanoparticles with Sea Water. *Science of the Total Environment*, **487**, 771-777. <http://dx.doi.org/10.1016/j.scitotenv.2013.11.082>
- [19] Sundaresan, V., Menon, J., Rahimi, M., Nguyen, K. and Wadajkar, A. (2014) Dual-Responsive Polymer-Coated Iron Oxide Nanoparticles for Drug Delivery and Imaging Applications. *International Journal Pharmaceutical*, **466**, 1-7. <http://dx.doi.org/10.1016/j.ijpharm.2014.03.016>
- [20] Jiang, H., Yan, Z., Zhao, Y., Hu, X. and Lian, H. (2012) Zincon-Immobilized Silica-Coated Magnetic Fe<sub>3</sub>O<sub>4</sub> Nanoparticles for Solid-Phase Extraction and Determination of Trace Lead in Natural and Drinking Waters by Graphite Furnace Atomic Absorption Spectrometry. *Talanta*, **94**, 251-256. <http://dx.doi.org/10.1016/j.talanta.2012.03.035>
- [21] Rho, W., Kim, H., Kyeong, S., Kang, Y., Kim, D., Kang, H., Jeong, C., Kim, D., Lee, Y. and Jun, B. (2014) Facile Synthesis of Monodispersed Silica-Coated Magnetic Nanoparticles. *Journal of Industrial and Engineering Chemistry*, **20**, 2646-2649. <http://dx.doi.org/10.1016/j.jiec.2013.12.014>
- [22] Sahoo, B., Sanjana, K., Devi, P., Dutta, S., Maiti, T., Pramanik, P. and Dhara, D. (2014) Biocompatible Mesoporous Silica-Coated Superparamagnetic Manganese Ferrite Nanoparticles for Targeted Drug Delivery and MR Imaging Applications. *Journal of Colloids and Interface Science*, **431**, 31-34. <http://dx.doi.org/10.1016/j.jcis.2014.06.003>
- [23] Khojastehnezhad, A., Rahimizadeh, M., Moeinpour, F., Eshghi, H. and Bakalovi, M. (2014) Polyphosphoric Acid Supported on Silica-Coated NiFe<sub>2</sub>O<sub>4</sub> Nanoparticles: An Efficient and Magnetically-Recoverable Catalyst for N-Formylation of Amines. *Comptes Rendus Chimie*, **17**, 459-464. <http://dx.doi.org/10.1016/j.crci.2013.07.013>
- [24] Chandra, S., Barick, K. and Bahadur, D. (2011) Oxide and Hybrid Nanostructures for Therapeutic Applications. *Advances in Drug Delivery Reviews*, **63**, 1267-128. <http://dx.doi.org/10.1016/j.addr.2011.06.003>
- [25] Ramanujan, R., Purushotham, S. and Chia, M. (2007) Processing and Characterization of Activated Carbon Coated Magnetic Nanoparticles for Biomedical Applications. *Materials Science and Engineering C*, **27**, 659-664. <http://dx.doi.org/10.1016/j.msec.2006.06.007>
- [26] Zhang, B., Xu, J., Xin, P., Han, Y., Hong, B., Jin, H., Peng, X., Li, J., Gong, J., Ge, H., Zhu, Z. and Wang, X. (2015)

- Magnetic Properties and Adsorptive Performance of Manganese-Zinc Ferrites/Activated Carbon Nanocomposites. *Journal of Solid State Chemistry*, **221**, 302-305. <http://dx.doi.org/10.1016/j.jssc.2014.10.020>
- [27] Rangel-Mendez, R. and Streat, M. (2002) Adsorption of Cadmium by Activated Carbon Cloth: Influence of Surface Oxidation and Solution pH. *Water Research*, **36**, 1244-1252. [http://dx.doi.org/10.1016/S0043-1354\(01\)00343-8](http://dx.doi.org/10.1016/S0043-1354(01)00343-8)
- [28] Múzquiz-Ramos, E., Guerrero-Chávez, V., Macías-Martínez, B., López-Badillo, C. and García-Cerda, L. (2015) Synthesis and Characterization of Maghemite Nanoparticles for Hyperthermia Applications. *Ceramics International*, **41**, 397-402. <http://dx.doi.org/10.1016/j.ceramint.2014.08.083>
- [29] Vitela-Rodríguez, A. and Rangel-Mendez, J. (2013) Arsenic Removal by Modified Activated Carbons with Iron Hydro (Oxide) Nanoparticles. *Journal of Environmental Management*, **114**, 225-231. <http://dx.doi.org/10.1016/j.jenvman.2012.10.004>
- [30] Decuzzi, P. and Ferrari, M. (2007) The Role of Specific and Non-Specific Interactions in Receptor-Mediated Endocytosis of Nanoparticles. *Biomaterials*, **28**, 2915-2922. <http://dx.doi.org/10.1016/j.biomaterials.2007.02.013>
- [31] Mendes, R., Koch, B., Bachmatiuk, A., El-Gendy, A., Krupskaya, Y., Springer, A., Klingeler, R., Schmidt, O., Buchner, B., Sanchez, S. and Rummeli, M. (2014) Synthesis and Toxicity Characterization of Carbon Coated Iron Oxide Nanoparticles with Highly Defined Size Distributions. *Biochimica et Biophysica Acta*, **1840**, 160-169. <http://dx.doi.org/10.1016/j.bbagen.2013.08.025>
- [32] Mangun, C. Berak, K., Daley, M. and Economy, J. (1999) Oxidation of Activated Carbon Fibers: Effect on Pore Size, Surface Chemistry and Adsorption Properties. *Chemistry of Materials*, **11**, 3476-3483. <http://dx.doi.org/10.1021/cm990123m>
- [33] Deatsch, A. and Evans, B. (2014) Heating Efficiency in Magnetic Nanoparticle Hyperthermia. *Journal of Magnetism and Magnetic Materials*, **354**, 163-172. <http://dx.doi.org/10.1016/j.jmmm.2013.11.006>
- [34] ASTM F756, Standard Practice for Assessment of Hemolytic Properties of Materials (2009) Annual Book of ASTM Standards. Committee F04 Medical and Surgical Materials and Devices, Subcommittee F04.16 Biocompatibility Test Methods.